Liquid-Liquid Transition in Kitaev Magnets Driven by Spin Fractionalization

Joji Nasu,[1] Yasuyuki Kato,[2] Junki Yoshitake,[2] Yoshitomo Kamiya,[3] and Yukitoshi Motome[2]

[1]*Department of Physics, Tokyo Institute of Technology, Meguro, Tokyo 152-8551, Japan*
[2]*Department of Applied Physics, University of Tokyo, Bunkyo, Tokyo 113-8656, Japan*
[3]*Condensed Matter Theory Laboratory, RIKEN, Wako, Saitama 351-0198, Japan*

(Dated: October 25, 2016)

While phase transitions between magnetic analogs of three states of matter — a long-range ordered state, paramagnet, and spin liquid — have been extensively studied, the possibility of "liquid-liquid" transitions, namely, between different spin liquids, remains elusive. By introducing the Ising coupling into the honeycomb Kitaev model with bond asymmetry, we discover that the Kitaev spin liquid becomes a bond-nematic quantum paramagnet before magnetically ordered. The phase transition between the two liquid-like states with different topological nature is of first order, driven by delocalization of the Z_2 gauge fluxes, and persists to a critical point at finite temperature located inside the regime where quantum spins are fractionalized. It is suggested that similar transitions may occur in other perturbed Kitaev magnets with bond asymmetry.

arXiv:1610.07343v1 [cond-mat.str-el] 24 Oct 2016

Quantum spin liquids (QSLs) have been the subject of great interest since Anderson's inspiring proposal [1]. In QSLs, localized spins do not solidify into a long-range magnetic order despite strong correlations even at zero temperature (T), analogous to a quantum fluid state of liquid helium. The intensively discussed candidates include some organic salts [2–4] and transition metal compounds [5–7] with geometric frustration. QSLs have brought as rich physics as done by liquid helium. For instance, topological orders can be used to characterize gapped QSLs [8, 9], in which fractionalization of quantum spins yields excitations of emergent statistics [10]. On the other hand, emergent fermionic excitations can be regarded as a hallmark of certain gapless QSLs, which has motivated investigating asymptotic low-T behavior of the specific heat and thermal conductivity [11, 12].

In his seminal work [13], Kitaev proposed the canonical model of QSLs, in which one can investigate its exotic properties without uncontrolled approximations. This simple $S = 1/2$ model with bond-dependent interactions provides exact realizations of QSLs with topological order and fractional excitations [13]. By introducing Majorana fermions, it can be shown that the ground state is a Z_2 QSL either gapped or gapless depending on the exchange parameters [14]. Moreover, exchange interactions in some transition metal compounds with strong spin-orbit coupling may be dominated by the Kitaev-type ones [15]. The exact solvability enables us to examine experimentally-accessible properties at both zero and finite T [16–24], providing a good starting point to understand QSLs and transitions into different phases.

In this Letter, we discuss the Kitaev model with additional interactions destabilizing the Kitaev QSL. Such extensions are in general important to describe real compounds that exhibit a long-range order at low T, though it poses a challenge as the exact solvability is lost. Indeed, following the pioneering work by Jackeli and Khaliullin [15], extensive theoretical efforts have been made on the Kitaev-Heisenberg and related models [25–36], where the Kitaev QSL is eventually replaced by some magnetically ordered phase. It has also been investigated how the proximity effects to the QSL are observed in the paramagnetic phase [36, 37]. However, other than such scenarios of obtaining conventional magnetic orders, a possibility of *nonmagnetic* phases distinct from the Kiteav QSLs has yet to be well explored. If such a liquid-like phase exists, the corresponding phase transition out of the Kitaev QSL is of particular interest as a magnetic analog of the "liquid-liquid" transition.

Specifically, we consider the honeycomb-lattice Kitaev-Ising model and show that a new liquid-like phase emerges as an intermediate phase when the Kitaev terms are bond-asymmetric and the anisotropy axis of the Ising coupling is orthogonal to that of the dominant Kitaev term. The ground-state phase diagram is obtained by using the exact diagonalization (ED) in finite-size clusters and the mean-field (MF) approximation in the Majorana fermion representation. We also investigate the finite-T properties using the thermal pure quantum (TPQ) state approach [38–41]. We show that the new nonmagnetic state is well described by a spin-nematic wavefunction without topological order. We find that the topological transition between the nematic and Kitaev QSL phases is discontinuous. The liquid-liquid transition line persisting at finite T terminates at a critical point. By bypassing the point, these two states are adiabatically connected through the peculiar paramagnet with fractionalized spin excitations, dubbed "fractionalized paramagnet." We will show that the fractionalization of quantum spins, in particular, delocalization of Z_2 gauge fluxes plays a major role in this transition.

The Hamiltonian of the Kitaev-Ising model is given by

$$\mathcal{H} = -\sum_{\gamma=x,y,z}\sum_{\langle jk\rangle_\gamma} J_\gamma \sigma_j^\gamma \sigma_k^\gamma - J_I \sum_{\langle jk\rangle} \sigma_j^z \sigma_k^z, \qquad (1)$$

where $\sigma_j^{x,y,z}$ denotes Pauli matrices representing the $S = 1/2$ spin at site j, J_γ is the Kitaev interaction on the γ-bond $\langle jk\rangle_\gamma$ of the honeycomb lattice [see Fig. 1(a)], and $J_I > 0$ is the ferromagnetic Ising coupling defined on all the nearest neighbors (NNs). For $J_I = 0$, gapped and gapless QSLs are stabilized depending on $J_{x,y,z}$ as shown in Fig. 1(b). We investigate not only the isotropic case $J_x = J_y = J_z$ [42] but also the range of anisotropy covering both gapped and gapless QSL regimes, using the ED and the MF approximation. Hereafter, we parametrize the Kitaev interactions as $J_x = 1 - 2\alpha/3$ and

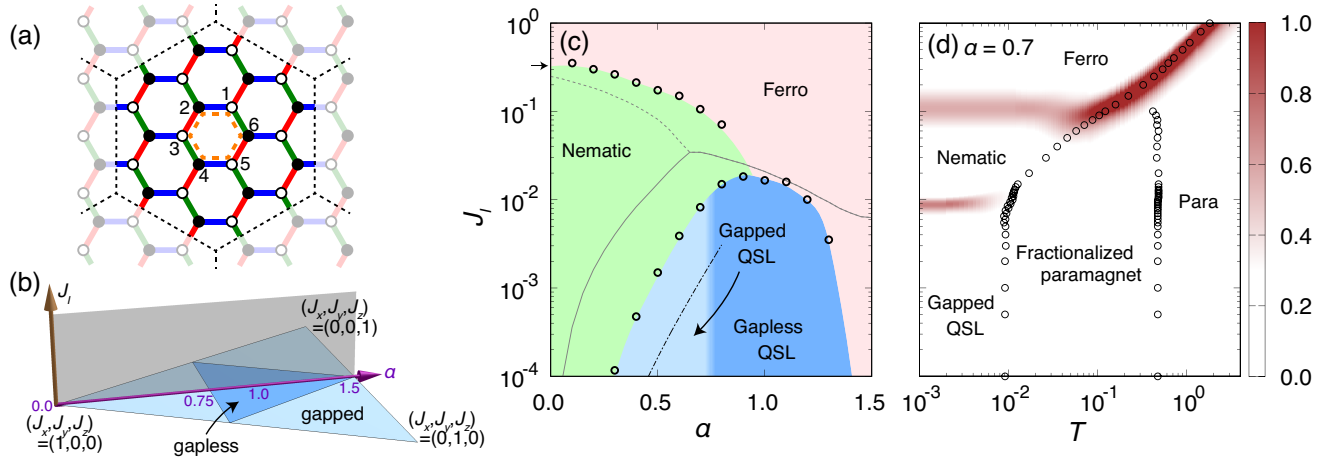

FIG. 1. (a) 24-site cluster of the honeycomb lattice with periodic boundary conditions, where blue, green, and red lines represent x-, y-, and z-bonds, respectively. The six-site loop with the dashed line represents $W_p = \sigma_1^z\sigma_2^y\sigma_3^x\sigma_4^z\sigma_5^y\sigma_6^x$. (b) Ground-state phase diagram of the pure Kitaev model on the basal plane of $J_x + J_y + J_z = 1$. The α- and the vertical axes parametrize the bond asymmetry (see the text) and J_I, respectively. (c) Ground-state phase diagram of the Kitaev-Ising model obtained by the ED at $T = 0$. The circles represent the phase boundary determined by the peaks of $-J_I d^2E/dJ_I^2$ (see Fig. 2). The dashed-dotted line shows the asymptotic phase boundary, $J_I = J_y^2J_z^2/(16J_x^3)$, between the Kitaev and the spin nematic liquids in the toric code limit. The small arrow on the vertical axis indicates the Ising transition point $J_I = 0.3258(1)$ for $\alpha = 0$. The solid (dotted) line shows the first- (second-)order phase boundary in the MF approximation. (d) Finite-T phase diagram at $\alpha = 0.7$ obtained by the TPQ state approach in the 24-site cluster in (a). The intensity map shows $-J_I d^2F/dJ_I^2$, the peaks of which imply the phase boundaries. The circles represent the peaks of the specific heat (see Fig. 3).

$J_y = J_z = \alpha/3$ taking $J_x + J_y + J_z = 1$ as the unit of energy ($J_\gamma \geq 0$). For $J_I = 0$, the gapless-gapped phase boundary is located at $\alpha = 3/4$.

Our ED and TPQ [38–40] studies have been performed in the 24-site cluster in Fig. 1(a). We also perform the MF calculation based on a Majorana fermion representation [42]. This is introduced by the Jordan-Wigner transformation along the chains comprising alternating x and y bonds by adopting the open boundary condition along these chains, leading to [43–45]

$$\mathcal{H} = -i\sum_{\gamma=x,y}\sum_{\langle jk\rangle_\gamma} J_\gamma c_j c_k + J_z\sum_{\langle jk\rangle_z} c_j c_k \bar{c}_j\bar{c}_k + J_I\sum_{\langle jk\rangle} c_j c_k\bar{c}_j\bar{c}_k, \quad (2)$$

where j and k denote sites on different sublattices represented by filled and open circles, respectively, in Fig. 1(a). c and $\bar{c}$ are the Majorana fermions at each site. For $J_I = 0$, $\bar{c}_j\bar{c}_k$ on each z bond commutes with $\mathcal{H}$, and hence, the Majorana fermions $\bar{c}$ are localized on z bonds giving rise to the static Z_2 gauge fields. We decouple the second and third terms in Eq. (2) by introducing MFs as $c_jc_k\bar{c}_j\bar{c}_k \to c_jc_k\langle\bar{c}_j\bar{c}_k\rangle + \langle c_jc_k\rangle\bar{c}_j\bar{c}_k - \langle c_jc_k\rangle\langle\bar{c}_j\bar{c}_k\rangle - c_j\bar{c}_j\langle c_k\bar{c}_k\rangle - \langle c_j\bar{c}_j\rangle c_k\bar{c}_k + \langle c_j\bar{c}_j\rangle\langle c_k\bar{c}_k\rangle - c_j\bar{c}_k\langle\bar{c}_jc_k\rangle - \langle c_j\bar{c}_k\rangle\bar{c}_jc_k + \langle c_j\bar{c}_k\rangle\langle\bar{c}_jc_k\rangle$, where $\langle\cdots\rangle$ are the thermal or the ground-state averages determined self-consistently.

Figure 1(c) shows the ground-state phase diagram on the (J_I, α) plane corresponding to the shaded plane in Fig. 1(b). For large enough J_I, a ferromagnetic phase appears as expected. Remarkably, however, between the QSL and the ferromagnetic phases, we find another nonmagnetic phase between the QSL and the ferromagnetic phase. Figure 2(a) shows the J_I-derivative of the ground state energy, $-dE/dJ_I$, evaluated with the ED calculation at $\alpha = 0.7$. It shows steeper slopes around $J_{Ic1} \sim 0.01$ and $J_{Ic2} \sim 0.1$, which can be more clearly seen as peaks in $-J_I d^2E/dJ_I^2$ [Fig. 2(b)]. Such peaks are known to be a good indicator of a phase transition [25], meaning that there are three phases separated by transitions at J_{Ic1} and J_{Ic2}.

To characterize these phases, first we calculate the mean square of the ferromagnetic order parameter $\langle m^2\rangle = \langle[(1/N)\sum_i \sigma_i^z]^2\rangle$ and $W = |\langle W_p\rangle|$, where $W_p = \sigma_1^z\sigma_2^y\sigma_3^x\sigma_4^z\sigma_5^y\sigma_6^x$ is the Z_2 flux on the plaquette p with the site indices shown in Fig. 1(a) [13]. For $J_I = 0$, the exact ground state corresponds to $W = 1$, while $\langle m^2\rangle \to 1$ is expected as $J_I \to \infty$ because of the ferromagnetic order. The J_I dependences of $\langle m^2\rangle$ and W for $\alpha = 0.7$ are presented in Fig. 2(c). W abruptly decreases from 1 to 0 around J_{Ic1} with increasing J_I, which implies that the topological order is lost at $J_I = J_{Ic1}$, whereas the rapid increase of $\langle m^2\rangle$ around J_{Ic2} implies the onset of the ferromagnetic long-range order. The Majorana fermion MF calculations yield qualitatively similar results [Figs. 2(e)–2(g)], and the topology of the MF phase diagram is the same as the ED results [Fig. 1(c)]. Hence, neither W nor $\langle m^2\rangle$ can fully characterize the intermediate phase in the range $J_{Ic1} < J < J_{Ic2}$, which thus should be neither the Kitaev QSL nor the magnetically ordered phase.

To clarify the nature of the intermediate phase, a key observation is that the new phase is widely extended in the small α regime ($J_x \gg J_\perp \equiv J_y = J_z$) especially for small J_I, as shown in Fig. 1(c). This suggests that one can analyze the nature by deriving an effective model in the anisotropic limit. As Kitaev demonstrated [13], such a large-J_x effective model for

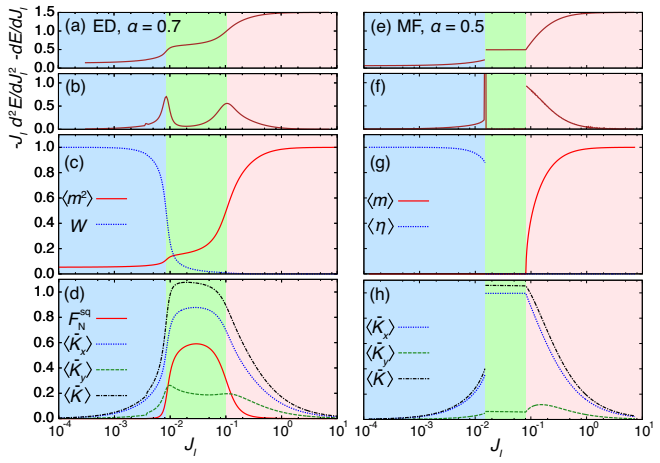

FIG. 2. (a)–(d) Ground state properties at $\alpha = 0.7$ obtained with the ED in the 24-site cluster shown in Fig. 1(a): (a) the first and (b) the second derivatives of the ground state energy in terms of J_I, (c) mean square of the magnetization $\langle m^2 \rangle$ and the flux density W, and (d) the dimensionless measures of kinetic energy of the Majorana fermions $\{\bar{c}_j\}$, $\langle \bar{K}_x \rangle$, $\langle \bar{K}_y \rangle$, $\langle \bar{K} \rangle = \langle \bar{K}_x \rangle + \langle \bar{K}_y \rangle$, and the squared fidelity $F_{\rm N}^{\rm sq}$ (see the text). (e)–(h) Majorana fermion MF results for the same or related observables (except for $F_{\rm N}^{\rm sq}$) for $\alpha = 0.5$: (e) $-dE/dJ_I$, (f) $-J_I d^2E/dJ_I^2$, (g) $\langle m \rangle = (1/N)\sum_i \langle \sigma_i^z \rangle$ and $\langle \eta \rangle = (2/N)\sum_{\langle ij \rangle_z} \langle \bar{c}_j \bar{c}_k \rangle$, and (h) $\langle \bar{K}_x \rangle$, $\langle \bar{K}_y \rangle$, and $\langle \bar{K} \rangle$. We note $W \approx \langle \eta \rangle^2$ in the MF approximation because of the relation $W_p = \eta_r \eta_{r'}$ for each plaquette p [43–45], where r, r' represent two z bonds of the plaquette p.

$J_I = 0$ is given by the toric code at the 4th order in $J_\perp$, which acts on the low-energy subspace spanned by direct products of $|\Rightarrow\rangle_{\langle jk \rangle_x} \equiv |{\rightarrow_j}{\rightarrow_k}\rangle$ and $|\Leftarrow\rangle_{\langle jk \rangle_x} \equiv |{\leftarrow_j}{\leftarrow_k}\rangle$ defined on each x-dimer with $|\rightarrow\rangle$ and $|\leftarrow\rangle$ being the eigenstates of σ^x with eigenvalues $+1$ and -1, respectively. With small nonzero J_I, the leading $O(J_I)$ contribution is to mutually flip $|\Rightarrow\rangle$ and $|\Leftarrow\rangle$ on each x dimer. Thus, to $O(J_\perp^4/J_x^3, J_I)$, the effective Hamiltonian is the toric code in an effective transverse field. This perturbative argument suggests that the instability of the gapped QSL for large J_x leads to a pseudospin polarized state well approximated by

$$|\psi_{\rm N}\rangle = \prod_{\langle jk \rangle_x} \frac{1}{\sqrt{2}} \left(|{\rightarrow_j}{\rightarrow_k}\rangle + |{\leftarrow_j}{\leftarrow_k}\rangle \right). \tag{3}$$

This is a *bond spin nematic* state [9] with its director pointing parallel to the y axis, where $\langle \psi_{\rm N} | \sigma_j^y \sigma_k^y | \psi_{\rm N} \rangle = -1$ on the x bonds in spite of the absence of the interaction of $\sigma_j^y \sigma_k^y$ on these bonds.

The spin nematic nature is indeed confirmed by computing the squared fidelity $F_{\rm N}^{\rm sq} = |\langle \psi_{\rm N} | \psi_{\rm gs} \rangle|^2$ of the ground-state wave function $|\psi_{\rm gs}\rangle$ relative to the proposed state $|\psi_{\rm N}\rangle$. As shown in Fig. 2(d), $F_{\rm N}^{\rm sq}$ obtained by ED shows a substantial nonzero value only for $J_{Ic1} < J_I < J_{Ic2}$, which indicates that the intermediate phase is the spin nematic phase.

Interestingly, $F_{\rm N}^{\rm sq}$ in the spin nematic phase is considerably reduced from the unity. The reduction is due to quantum corrections induced by the next-to-leading $O(J_\perp J_I/J_x)$ and higher order effects [46], which also result in nonnegligible expectation values of not only $\bar{K}_x = -(2/N)\sum_{\langle jk \rangle_x} \sigma_j^y \sigma_k^y$ but also $\bar{K}_y = -(2/N)\sum_{\langle jk \rangle_y} \sigma_j^x \sigma_k^x$, as shown in Fig. 2(d). These are the dimensionless measures of the kinetic energy of the Majorana fermions $\{\bar{c}_j\}$ because $\bar{K}_{x(y)} = (2/N)\sum_{\langle jk \rangle_{x(y)}} i\bar{c}_j \bar{c}_k$. Such enhanced kinetic energy of $\{\bar{c}_j\}$ is also captured by the Majorana fermion MF calculation as shown in Fig. 2(h). Since $\{\bar{c}_j\}$ are completely localized in the Kitaev limit, the substantial enhancement of $\bar{K}_{x,y}$ suggests that the first-order liquid-liquid transition is driven by delocalization of the Z_2 gauge fluxes. This picture will be confirmed by finite-T calculations later.

As for the nature of the QSL-nematic transition, the mapping to the transverse-field toric code allows us to conclude that it should be of first order, at least, in the large J_x limit [47]. Indeed, our MF calculation indicates the first-order nature [see Figs. 2(e) and 2(f)], and our ED results also show a rather sharp change in the energy at the phase boundary [Figs. 2(a) and 2(b)]. The asymptotic phase boundary in the large J_x limit can be predicted as $J_I \sim J_y^2 J_z^2/(16 J_x^3)$ based on the previous work on the transverse-field toric code [47], which is plotted by the dashed-dotted line in Fig. 1(c). The deviation of our ED results from this expected behavior can be accounted for as the finite-size effect [46]. The results indicate that our Kitaev-Ising model exhibits the first-order liquid-liquid transition from the Kitaev QSL to the spin nematic phase with losing topological nature.

On the other hand, both the ED [Figs. 2(a) and 2(b)] and the MF approximation [Figs. 2(e) and 2(f)] indicate a continuous transition between the spin nematic and the ferromagnetic phases. For $J_y = 0$ and $J_I > 0$, we can show that the Hamiltonian is reduced to a two-dimensional transverse-field Ising model to describe this phase transition at $T = 0$ [46]. The analysis predicts that the continuous transition takes place at $J_I = 0.3285(1)$ at $\alpha = 0$ ($J_y = J_z = 0$), which is consistent with the ED results [see Fig. 1(c)].

The two phase transitions extend to finite T in the following manner. We determine the finite-T phase diagram [Fig. 1(d)] from the extension of the argument in Fig. 2(b), namely, by calculating $-J_I d^2F/dJ_I^2$ (F is the free energy). We here obtain the second derivative by numerically differentiating $dF/dJ_I = -(1/N)\sum_{\langle jk \rangle} \langle \sigma_j^z \sigma_k^z \rangle$ evaluated with the TPQ state approach. As shown in Fig. 1(d), the ferromagnetic phase is surrounded by the peak of $-J_I d^2F/dJ_I^2$ associated with the symmetry breaking. On the other hand, the peak emanating from the first-order QSL-nematic quantum transition disappears around $(J_I, T) \sim (0.01, 0.002)$, indicating that the liquid-liquid transition line terminates at this critical point.

Notably, the end point lies well inside the "fractionalized paramagnet" inherited from the pure Kitaev model. In contrast to the trivial paramagnet, it exhibits fermionic excitations out of thermal fractionalization of quantum spins, which is signaled by successive crossovers each releasing a half of the spin entropy [21]. The successive crossovers are observed in the Kitaev-Ising model. Figures 3(a) and 3(d) show the T dependences of the specific heat at $J_I = 0.001$ and $J_I = 0.03$, at which the ground states are the Kitaev QSL and the nematic

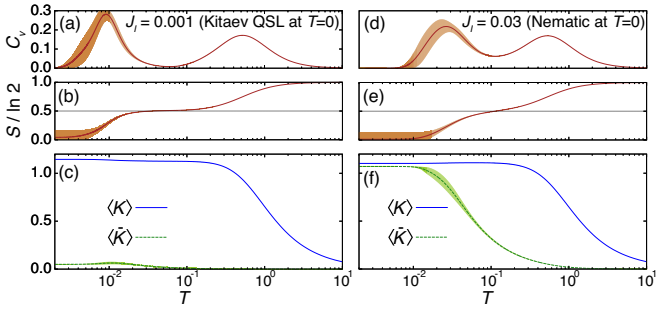

FIG. 3. (a)–(c) T dependences of (a) the specific heat, (b) normalized entropy, and (c) the dimensionless measures of kinetic energy $\langle K\rangle$ and $\langle\bar{K}\rangle$ of $\{c_j\}$ and $\{\bar{c}_j\}$, respectively, at $J_I = 0.001$ and $\alpha = 0.7$, where the ground state is the Kitaev QSL. (d)–(f) Corresponding data for $J_I = 0.03$ and $\alpha = 0.7$, where the ground state is spin nematic. The shaded broadening represents errors associated with the TPQ state approach.

spin liquid, respectively. Both of them show two broad peaks and the entropy release associated with each is the half of the total [Figs. 3(b) and 3(e)]. As shown in Fig. 1(d), the end point is well below the line of the higher peak temperature ($T \sim 0.1$) where the fractionalization sets in as decreasing T. Thus, the two liquid regions, both of which preserves the global symmetry of $\mathcal{H}$, are adiabatically connected at finite T through the fractionalized paramagnetic regime by bypassing the critical point.

The thermal fractionalization is known to enhance the kinetic energy of the Majorana fermions $\{c_j\}$ below the high-T crossover. In the spin language, this corresponds to development of the NN spin correlation, as found in the pure Kitaev model [20, 21]. We confirm this behavior by calculating its dimensionless measure, $K = (2/N)\sum_{\gamma=x,y}\sum_{\langle jk\rangle_\gamma}\sigma_j^\gamma\sigma_k^\gamma = (2/N)\sum_{\gamma=x,y}\sum_{\langle jk\rangle_\gamma} ic_jc_k$, regardless of whether the ground state is the Kitaev QSL [Fig. 3(c)] or the spin nematic liquid [Fig. 3(f)].

On the other hand, the low-T crossover corresponds to the emergence of the distinct characterizations of the two liquids, and the appearance of the critical point and the subsequent first-order phase boundary are its direct consequences. Here, the Majorana fermions $\{\bar{c}_j\}$ take the leading role. To see this, we show the dimensionless measure of their kinetic energy $\bar{K} = \bar{K}_x + \bar{K}_y$ with $\bar{K}_{x,y}$ defined previously. When the ground state is the Kitaev QSL, $\langle\bar{K}\rangle$ is very small at any T [Fig. 3(c)]. On the other hand, when the ground state is spin nematic, while $\langle K\rangle$ exhibits similar T dependence as above, $\langle\bar{K}\rangle$ starts to develop around the lower crossover temperature [Fig. 3(f)]. This indicates that the two spin liquids are of different origins, as discussed above for $T = 0$: While the Majorana fermions $\{\bar{c}_j\}$ are localized at any T in the Kitaev QSL, they become delocalized in the spin nematic liquid below the low-T crossover. The itinerant behavior of $\{\bar{c}_j\}$ originates from the Fock term of the Ising interaction, $\langle c_jc_k\rangle\bar{c}_j\bar{c}_k$, in the MF picture. This is consistent with the fact that the lower crossover temperature increases with J_I almost linearly in the nematic case, whereas it exhibits weak J_I dependence in the Kitaev QSL regime, as shown in Fig. 1(d). Thus, separated by the first-order transition line, $\{\bar{c}_j\}$ are localized (delocalized) for smaller (larger) J_I, indicating that the driving force of the transition is the delocalization of emergent fractional particles $\{\bar{c}_j\}$.

We note that the above arguments can be rationalized based on the mapping to the transverse-field toric code. This effective model has a finite-T phase diagram of the same structure featuring a termination of a first-order phase boundary persisting from $T = 0$. This was concluded after a yet another mapping via the Xu-Moore model for the $p + ip$ superconductor arrays [48] to the quantum compass model on a square lattice [49], where numerical studies found the critical point to be in the 2D Ising universality class [50, 51].

In summary, we investigated the Kitaev-Ising model at both zero and finite T and found the liquid-liquid transition between the Kitaev QSL and the newly-identified spin nematic phases. The QSL-nematic transition is of first order, driven by the delocalization of the Z_2 gauge fluxes. The two liquids can be distinguished at $T = 0$ in terms of topological order but are continuously connected at finite T through the fractionalized paramagnetic regime. We emphasize that the Kitaev-Ising Hamiltonian is not a prerequisite for the proposed liquid-liquid transition; similar transitions are expected to occur in other extended Kitaev models, such as the Kitaev-Heisenberg model and the J-K-Γ model, with large bond asymmetry [52]. We hope our work will promote further studies for unveiling new quantum phases proximate to the Kitaev QSL and stimulate experimental efforts on candidate materials.

This work is supported by Grant-in-Aid for Scientific Research under Grant No. JP24340076, JP26800199, JP15K13533, JP16K17747, and JP16H02206. Parts of the numerical calculations are performed in the supercomputing systems in ISSP, the University of Tokyo. The calculations by TPQ states have been performed using the $\mathcal{H}\Phi$ package [41].

—Supplemental Material—

I. Finite-size effect near the QSL-nematic transition

In this section, we explain the origin of the rather strong finite-size effect seen in the QSL-nematic transition in Fig. 1(c) in the main text. While this transition can be best understood through the mapping to the transverse-field toric code model as discussed in the main text, additional topological boundary terms appear in finite-size clusters from the perturbation processes passing through the boundary of the cluster. The additional terms are also conserved quantities at $J_I = 0$ as the usual toric code terms, hence lowering the ground state energy in the QSL phase. Consequently, it is expected that the QSL region can be overestimated in finite-size

TABLE SI. The dimer-site indices R_1–R_4 contributing to $\mathcal{H}^{R_1R_2R_3R_4}_{\text{eff, boundary (1)}}$ in Eq. (S4).

R_1	R_2	R_3	R_4
1	3	6	10
2	4	7	11
6	5	8	12
7	10	9	3
8	11	1	4
9	12	2	5
3	6	5	9
4	7	10	1
5	8	11	2
10	9	12	6
11	1	3	7
12	2	4	8

clusters. Below we confirm this expectation, showing explicitly that the strong finite-size effect exists in the $N = 24$ cluster [Fig. 1(a)] used to construct our phase diagram in the main text, due to such boundary terms appearing at the same order as the usual toric code terms.

We assume $J_x \gg J_\perp \equiv J_y = J_z \gg J_I > 0$. In the thermodynamic limit, the effective Hamiltonian to $O(J_\perp^4/J_x^3, J_\perp J_I/J_x)$ comprises the four-pseudospin toric code term J_{TC}, the effective transverse field term h_{eff}, and the Ising term J_z^τ on the y bonds, as

$$\mathcal{H}_{\text{eff, bulk}} = -J_{\text{TC}} \sum_R \tau^y_R \tau^z_{R+\mathbf{a}} \tau^y_{R+\mathbf{a}+\mathbf{b}} \tau^z_{R+\mathbf{b}} - h_{\text{eff}} \sum_R \tau^x_R + J_z^\tau \sum_R \tau^z_R \tau^z_{R+\mathbf{b}} + c(J_x, J_\perp, J_I), \tag{S1}$$

with $J_{\text{TC}} = J_\perp^4/(16J_x^3)$ [13], $h_{\text{eff}} = J_I$, and $J_z^\tau = J_\perp J_I/(2J_x)$, where R runs over the J_x dimers. $\tau^{x,y,z}$ are the pseudospin Pauli matrices acting on the low-energy subspace spanned by direct products of $|\Rightarrow\rangle_R \equiv |\rightarrow\rightarrow\rangle_R$ and $|\Leftarrow\rangle_R \equiv |\leftarrow\leftarrow\rangle_R$, namely,

$$\tau^z = \begin{pmatrix} 1 & 0 \\ 0 & -1 \end{pmatrix}, \quad \tau^x = \begin{pmatrix} 0 & 1 \\ 1 & 0 \end{pmatrix}, \quad \tau^y = \begin{pmatrix} 0 & -i \\ i & 0 \end{pmatrix}, \tag{S2}$$

in this dimer basis. For $J_I = 0$, the ground state energy per unit cell (of the honeycomb lattice) is $E^{J_I=0}_{\text{eff, bulk}} = -J_{\text{TC}} + O(J_\perp^6/J_x^5)$ apart from the constant term in Eq. (S1),

$$c(J_x, J_\perp, J_I) = -J_x - J_\perp^2/(4J_x) - (J_\perp^2 + 2J_\perp J_I)/(4J_x) + J_\perp^4/(32J_x^3) + O(J_\perp^6/J_x^5, (J_\perp/J_x)^2 J_I). \tag{S3}$$

For $J_z^\tau = 0$, the Hamiltonian (S1) coincides with the transverse-field toric code studied in Ref. [47].

In the $N = 24$ cluster shown in Fig. 1(a) or Fig. S1, there are additional contributions at the same order as the toric code terms arising from the perturbation processes through the boundary of the cluster, as illustrated in Figs. S1(a) and S1(b). The perturbation corresponding to Fig. S1(a) gives rise to the additional term,

$$\mathcal{H}^{R_1R_2R_3R_4}_{\text{eff, boundary (1)}} = 5J_{\text{TC}} \tau^y_{R_1} \tau^x_{R_2} \tau^y_{R_3} \tau^x_{R_4}, \tag{S4}$$

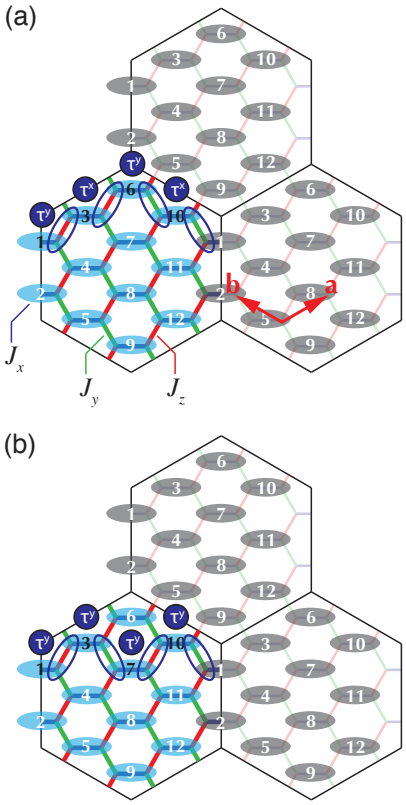

FIG. S1. Schematic pictures of the additional perturbation processes in the $N = 24$ cluster. (a) and (b) correspond to Eqs. (S4) and (S5), respectively. See Tables SI and SII for the complete lists of the dimers belonging to the categories (a) and (b), respectively.

TABLE SII. The dimer-site indices R_1–R_4 contributing to $\mathcal{H}^{R_1R_2R_3R_4}_{\text{eff, boundary (2)}}$ in Eq. (S5).

R_1	R_2	R_3	R_4
1	3	7	10
2	4	8	11
6	5	9	12
3	6	10	9
4	7	11	1
5	8	12	2

where R_1–R_4 are the dimer sites contributing the perturbation process; we summarize the list of R_1–R_4 in Table SI. Similarly, the perturbation corresponding to Fig. S1(b) leads to

$$\mathcal{H}^{R_1R_2R_3R_4}_{\text{eff, boundary (2)}} = -5J_{\text{TC}} \tau^y_{R_1} \tau^y_{R_2} \tau^y_{R_3} \tau^y_{R_4}, \tag{S5}$$

with the associated sites R_1–R_4 in this category are summarized in Table SII. All of these additional terms (18 terms in total) are conserved binary quantities, which we call the topological boundary terms. Thus, the ground state energy density

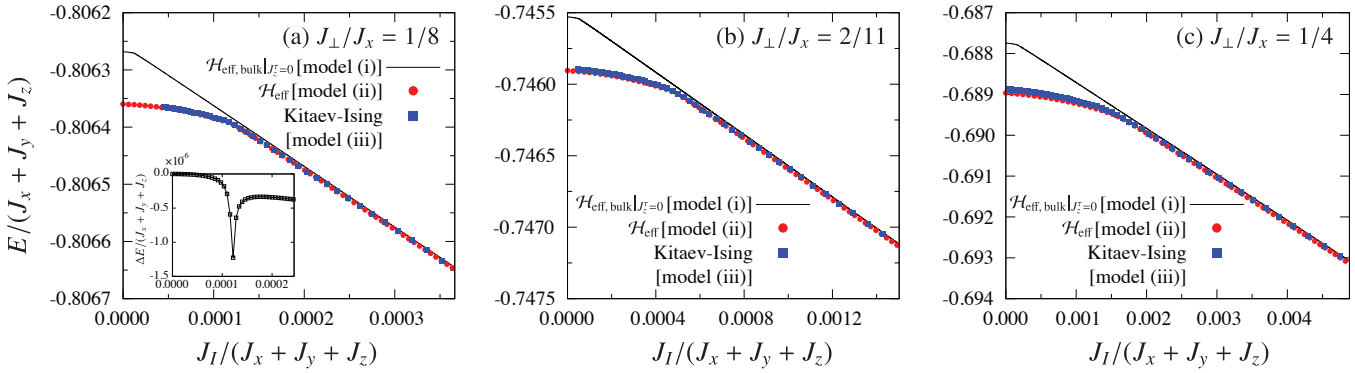

FIG. S2. Ground-state energy density E for (a) $J_\perp/J_x = 1/8$, (b) $J_\perp/J_x = 2/11$, and (c) $J_\perp/J_x = 1/4$ ($\alpha = 0.3$, 0.4, and 0.5, respectively) evaluated with the different approaches (i)–(iii) (see the text). The inset in (a) shows the change $\Delta E = E|_{J_z^\tau\neq 0} - E|_{J_z^\tau=0}$ induced by the J_z^τ term in the extended toric code Hamiltonian in a transverse magnetic field [Eq. (S1)].

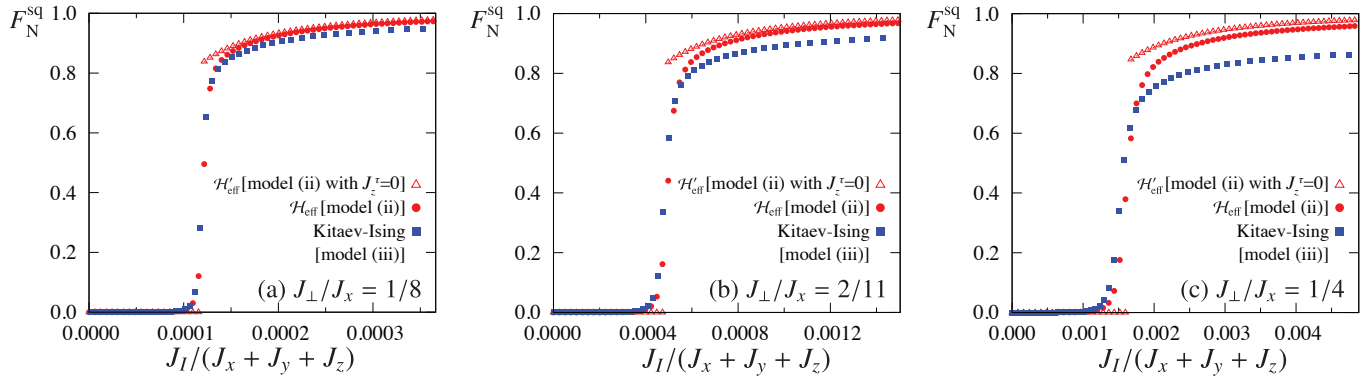

FIG. S3. Squared fidelity F_{N}^{sq} of the ground state with respect to the direct product of the bond nematic states (see the text and Eq. (3) of the main text). We show the comparisons among two variants of the approach (ii), namely, $\mathcal{H}_{\text{eff}}$ and $\mathcal{H}'_{\text{eff}}$ (see the text), and the Kitaev-Ising model for (a) $J_\perp/J_x = 1/8$, (b) $J_\perp/J_x = 2/11$, and (c) $J_\perp/J_x = 1/4$ ($\alpha = 0.3$, 0.4, and 0.5, respectively).

in this cluster at $J_I = 0$ is lowered by

$$\Delta E_{\text{eff, bulk}}^{J_I=0} = -\frac{15}{2} J_{\text{TC}} + O(J_\perp^6/J_x^5), \tag{S6}$$

which in fact dominates the bulk contribution from Eq. (S1).

In Fig. S2, we compare the ground state energy per unit cell for several values of $J_\perp/J_x$ as a function of J_I evaluated with different approaches: (i) the 10th-order perturbation theory presented in Ref. [47] for the transverse-field toric code model $\mathcal{H}_{\text{eff, bulk}}|_{J_z^\tau=0}$, which is expected to be accurate enough (the J_z^τ term gives a negligible contribution as discussed later), (ii) the effective Hamiltonian including the topological boundary terms $\mathcal{H}_{\text{eff}} = \mathcal{H}_{\text{eff, bulk}} + \sum_{(R_1,R_2,R_3,R_4)} \mathcal{H}_{\text{eff, boundary (1)}}^{R_1R_2R_3R_4} + \sum_{(R_1,R_2,R_3,R_4)} \mathcal{H}_{\text{eff, boundary (2)}}^{R_1R_2R_3R_4}$ for $N/2 = 12$ pseudospins derived from the $N = 24$ cluster, and (iii) the original Kitaev-Ising model on the $N = 24$ cluster. We find that for all the cases shown in Figs. S2(a)–S2(c), the results of (ii) and (iii) agree very well with each other, demonstrating the validity of our strong coupling approach including the topological boundary terms. Meanwhile, these results largely deviate from the bulk effective model (i) especially in the Kitaev QSL region for small J_I, where their ground state energies are lowered because of the boundary effect. In the main text, the phase boundary between the QSL and the spin-nematic phases is estimated from the first peak in $-J_I d^2E/dJ_I^2$ [see Fig. 2(b)], which corresponds to the kinks seen in E as a function of J_I in Figs. S2(a)–S2(c). Because E turns out to be almost insensitive to the boundary effect in the spin-nematic phase for large J_I, the lowering of the energy in (ii) and (iii) for small J_I results in the shift of the critical point estimated in the present finite-size cluster to larger values of J_I, hence overestimating the QSL phase.

However, because the boundary terms like Eqs. (S4) and (S5) become increasingly higher order corrections on larger clusters and thus are negligible in the thermodynamic limit, this result indicates that Eq. (S1) is a very good effective theory in the regime of the QSL-nematic transition. Thus, the asymptotic form of the QSL-nematic phase boundary mentioned in the main text corresponds to not the kinks in (ii) or (iii) but rather to the one in (i) in Fig. S2.

We note that the effect of the additional J_z^τ term is almost negligible in usual observables like energy. Indeed, the same degree of agreement can be achieved also by considering $\mathcal{H}'_{\rm eff} \equiv \mathcal{H}_{\rm eff}\big|_{J_z^\tau=0} = \mathcal{H}_{\rm eff,\,bulk}\big|_{J_z^\tau=0} + \sum_{(R_1,R_2,R_3,R_4)} \mathcal{H}^{R_1R_2R_3R_4}_{\rm eff,\,boundary\,(1)} + \sum_{(R_1,R_2,R_3,R_4)} \mathcal{H}^{R_1R_2R_3R_4}_{\rm eff,\,boundary\,(2)}$, as illustrated in the inset of Fig. S2(a).

On the other hand, the J_z^τ term and even higher order corrections are important to reproduce the behavior of the squared fidelity $F_{\rm N}^{\rm sq}$ in the Kitaev-Ising model (see Fig. S3). Here, $F_{\rm N}^{\rm sq}$ in the pseudospin language is defined as $F_{\rm N}^{\rm sq} = |\langle\psi_{\rm N}{}'|\psi_{\rm gs}\rangle|^2$ where $|\psi_{\rm N}{}'\rangle = \prod_R (1/\sqrt{2})(|\Rightarrow\rangle_R + |\Leftarrow\rangle_R)$ and $|\psi_{\rm gs}\rangle$ is the ground state wavefunction. It is found that $F_{\rm N}^{\rm sq}$ in the spin nematic phase of the Kitaev-Ising model is more reduced than that of the transverse-field toric code for $J_z^\tau = 0$ with the finite-size term ($\mathcal{H}_{\rm eff}|_{J_z^\tau=0}$) and the J_z^τ term modifies $F_{\rm N}^{\rm sq}$ in the right direction in the effective model. Still, discrepancies are left, which are more significant for larger values of α, implying that $F_{\rm N}^{\rm sq}$ is sensitive to the accuracy of the effective model description.

II. Reduced model for the nematic-magnetic transition

To discuss the transition between the spin nematic and the ferromagnetic phases, we construct a reduced model assuming $J_y = 0$ and $J_I > 0$. In this case, $\sigma_j^z\sigma_k^z$ on each x bond is conserved, and the reduced Hamiltonian is block-diagonalized in subspaces specified by the eigenvalues of $\sigma_j^z\sigma_k^z$ on each x bond. By introducing a new x-bond basis $|\tilde{\uparrow}\rangle_{\langle jk\rangle_x} = |\uparrow_j\uparrow_k\rangle$ ($|\uparrow_j\downarrow_k\rangle$) and $|\tilde{\downarrow}\rangle_{\langle jk\rangle_x} = |\downarrow_j\downarrow_k\rangle$ ($|\downarrow_j\uparrow_k\rangle$) for $\sigma_j^z\sigma_k^z = +1\,(-1)$ on each x-bond $R = \langle jk\rangle_x$ (here $|\uparrow\rangle$ and $|\downarrow\rangle$ are the eigenstates of σ^z) and the pseudospin $\tilde{\boldsymbol{\tau}}_R$ for these states, the Hamiltonian in a subspace V characterized by a configuration of $\{\sigma_j^z\sigma_k^z = \pm 1\}$ for x bonds is given by

$$\mathcal{H}^V_{\rm eff} = \tilde{\mathcal{H}}^V_{\rm eff} + \tilde{E}^V, \tag{S7}$$

where

$$\tilde{\mathcal{H}}^V_{\rm eff} = -J_I \sum_{\langle RR'\rangle_y} c^V_{RR'}\tilde{\tau}^z_R\tilde{\tau}^z_{R'} - (J_z + J_I)\sum_{\langle RR'\rangle_z} c^V_{RR'}\tilde{\tau}^z_R\tilde{\tau}^z_{R'} - J_x\sum_R(\tilde{\tau}^x_R + 1), \tag{S8}$$

$$\tilde{E}^V = -J_I\left(\frac{N}{2} - 2n\right) + \frac{J_xN}{2}. \tag{S9}$$

Here, $\langle RR'\rangle_y$ ($\langle RR'\rangle_z$) stands for a NN x-dimer sites connected by a y (z) bond, and n is the number of x bonds with $\sigma_j^z\sigma_k^z = -1$. The coefficient $c^V_{RR'}$ taking ±1 for each y or z bond is given by $c^V_{RR'} = \langle\psi^V_{\rm up}|\sigma_j^z\sigma_k^z|\psi^V_{\rm up}\rangle$, where j and k are NN sites on the corresponding y or z bond of the original honeycomb lattice and $|\psi^V_{\rm up}\rangle = \prod_R|\tilde{\uparrow}\rangle_R$, which depends on V in terms of bases written by $|\uparrow\rangle$ and $|\downarrow\rangle$. Particularly, all $c^V_{RR'}$ take $+1$ in the subspace with $\sigma_j^z\sigma_k^z = +1$ for all x bonds. We term this subspace V_m hereafter.

In the matrix representation on the basis of the direct product states $|\tilde{\rightarrow}\rangle_R = \frac{1}{\sqrt{2}}(|\tilde{\uparrow}\rangle + |\tilde{\downarrow}\rangle)_R$ and $|\tilde{\leftarrow}\rangle_R = \frac{1}{\sqrt{2}}(|\tilde{\uparrow}\rangle - |\tilde{\downarrow}\rangle)_R$, all matrix elements of $\tilde{\mathcal{H}}^{V_m}_{\rm eff}$ are negative. Using the relation $\sum_{ij} v_i^*A_{ij}v_j/|\boldsymbol{v}|^2 \geq \sum_{ij}|v_i|(-|A_{ij}|)|v_j|/|\boldsymbol{v}|^2$ for an arbitrary Hermitian matrix A and vector $\boldsymbol{v}$, we find that the ground state energy of $\tilde{\mathcal{H}}^{V_m}_{\rm eff}$ is the smallest. Moreover, $\tilde{E}^V$, which is constant in each subspace, is the smallest for the subspace V_m. Thus, the ground state is always in the subspace V_m.

Finally we obtain the two-dimensional transverse-field Ising model after the projection to the subspace V_m,

$$\mathcal{H}^{V_m}_{\rm eff} = -J_I\sum_{\langle RR'\rangle_y}\tilde{\tau}^z_R\tilde{\tau}^z_{R'} - (J_z + J_I)\sum_{\langle RR'\rangle_z}\tilde{\tau}^z_R\tilde{\tau}^z_{R'} - J_x\sum_R\tilde{\tau}^x_R - \frac{J_IN}{2}. \tag{S10}$$

This model undergoes a second-order phase transition between the ferromagnetic phase $\langle\tilde{\tau}^z\rangle \neq 0$ and the quantum paramagnet with $\langle\tilde{\tau}^z\rangle = 0$, which corresponds to the spin-nematic liquid. Indeed, our MF results show a continuous transition, as shown in Fig. 1(c) and Figs. 2(e)–2(f) of the main text. Particularly, the case with $J_y = J_z = 0$ is mapped to the quantum Ising model on the perfect square lattice, in which case the quantum critical point is at $J_I = 1/3.044(1)$ [53], as indicated by the small arrow on the vertical axis in Fig. 1(c) of the main text. The result is consistent with our ED results. We therefore conclude that the transition from the spin nematic to ferromagnetic phase is of second order.

[1] P. Anderson, Resonating valence bonds: A new kind of insulator?, Mater. Res. Bull. **8**, 153 (1973).

[2] Y. Shimizu, K. Miyagawa, K. Kanoda, M. Maesato, and G. Saito, Spin Liquid State in an Organic Mott Insulator with a Triangular Lattice, Phys. Rev. Lett. **91**, 107001 (2003).

[3] M. Yamashita, N. Nakata, Y. Senshu, M. Nagata, H. M. Yamamoto, R. Kato, T. Shibauchi, and Y. Matsuda, Highly Mobile Gapless Excitations in a Two-Dimensional Candidate Quantum Spin Liquid, Science **328**, 1246 (2010).

[4] T. Isono, H. Kamo, A. Ueda, K. Takahashi, M. Kimata, H. Tajima, S. Tsuchiya, T. Terashima, S. Uji, and H. Mori, Gapless Quantum Spin Liquid in an Organic Spin-1/2 Triangular-Lattice $\kappa - H_3$(Cat-EDT-TTF)$_2$, Phys. Rev. Lett. **112**, 177201 (2014).

[5] S. Nakatsuji, Y. Nambu, H. Tonomura, O. Sakai, S. Jonas, C. Broholm, H. Tsunetsugu, Y. Qiu, and Y. Maeno, Spin disorder on a triangular lattice, Science **309**, 1697 (2005).

[6] J. S. Helton, K. Matan, M. P. Shores, E. A. Nytko, B. M. Bartlett, Y. Yoshida, Y. Takano, A. Suslov, Y. Qiu, J.-H. Chung, D. G. Nocera, and Y. S. Lee, Spin Dynamics of the Spin-1/2 Kagome Lattice Antiferromagnet $ZnCu_3(OH)_6Cl_2$, Phys. Rev. Lett. **98**, 107204 (2007).

[7] Y. Okamoto, M. Nohara, H. Aruga-Katori, and H. Takagi, Spin-Liquid State in the $S = 1/2$ Hyperkagome Antiferromagnet $Na_4Ir_3O_8$, Phys. Rev. Lett. **99**, 137207 (2007).

[8] X.-G. Wen, Quantum Field Theory of Many-Body Systems (Oxford University Press, Oxford, 2004).

[9] C. Lacroix, P. Mendels, and F. Mila, Introduction to Frustrated Magnetism, Springer Series in Solid-State Sciences (Springer, Heidelberg, 2011).

[10] M. Oshikawa and T. Senthil, Fractionalization, Topological Order, and Quasiparticle Statistics, Phys. Rev. Lett. **96**, 060601 (2006).

[11] S. Yamashita, Y. Nakazawa, M. Oguni, Y. Oshima, H. Nojiri, Y. Shimizu, K. Miyagawa, and K. Kanoda, Thermodynamic properties of a spin-1/2 spin-liquid state in a κ-type organic salt, Nature Physics **4**, 459 (2008).

[12] M. Yamashita, N. Nakata, Y. Kasahara, T. Sasaki, N. Yoneyama, N. Kobayashi, S. Fujimoto, T. Shibauchi, and Y. Matsuda, Thermal-transport measurements in a quantum spin-liquid state of the frustrated triangular magnet-(BEDT-TTF)$_2$Cu$_2$(CN)$_3$, Nat. Phys. **5**, 44 (2009).

[13] A. Kitaev, Anyons in an exactly solved model and beyond, Ann. Phys. (N. Y.) **321**, 2 (2006).

[14] G. Baskaran, S. Mandal, and R. Shankar, Exact Results for Spin Dynamics and Fractionalization in the Kitaev Model, Phys. Rev. Lett. **98**, 247201 (2007).

[15] G. Jackeli and G. Khaliullin, Mott Insulators in the Strong Spin-Orbit Coupling Limit: From Heisenberg to a Quantum Compass and Kitaev Models, Phys. Rev. Lett. **102**, 017205 (2009).

[16] J. Knolle, D. L. Kovrizhin, J. T. Chalker, and R. Moessner, Dynamics of a Two-Dimensional Quantum Spin Liquid: Signatures of Emergent Majorana Fermions and Fluxes, Phys. Rev. Lett. **112**, 207203 (2014).

[17] J. Knolle, G.-W. Chern, D. L. Kovrizhin, R. Moessner, and N. B. Perkins, Raman Scattering Signatures of Kitaev Spin Liquids in A_2IrO$_3$ Iridates with A = Na or Li, Phys. Rev. Lett. **113**, 187201 (2014).

[18] B. Perreault, J. Knolle, N. B. Perkins, and F. J. Burnell, Theory of Raman response in three-dimensional Kitaev spin liquids: Application to β- and $\gamma - Li_2IrO_3$ compounds, Phys. Rev. B **92**, 094439 (2015).

[19] J. Knolle, D. L. Kovrizhin, J. T. Chalker, and R. Moessner, Dynamics of fractionalization in quantum spin liquids, Phys. Rev. B **92**, 115127 (2015).

[20] J. Nasu, M. Udagawa, and Y. Motome, Vaporization of Kitaev Spin Liquids, Phys. Rev. Lett. **113**, 197205 (2014).

[21] J. Nasu, M. Udagawa, and Y. Motome, Thermal fractionalization of quantum spins in a Kitaev model: Temperature-linear specific heat and coherent transport of Majorana fermions, Phys. Rev. B **92**, 115122 (2015).

[22] J. Nasu and Y. Motome, Thermodynamics of Chiral Spin Liquids with Abelian and Non-Abelian Anyons, Phys. Rev. Lett. **115**, 087203 (2015).

[23] J. Yoshitake, J. Nasu, and Y. Motome, Fractional Spin Fluctuation as a Precursor of Quantum Spin Liquids: Majorana Dynamical Mean-Field Study for the Kitaev Model, preprint , arXiv:1602.05253 (unpublished).

[24] J. Nasu, J. Knolle, D. L. Kovrizhin, Y. Motome, and R. Moessner, Fermionic response from fractionalization in an insulating two-dimensional magnet, Nat. Phys. **12**, 912 (2016).

[25] J. Chaloupka, G. Jackeli, and G. Khaliullin, Kitaev-Heisenberg Model on a Honeycomb Lattice: Possible Exotic Phases in Iridium Oxides A_2IrO$_3$, Phys. Rev. Lett. **105**, 027204 (2010).

[26] J. Chaloupka, G. Jackeli, and G. Khaliullin, Zigzag Magnetic Order in the Iridium Oxide Na$_2$IrO$_3$, Phys. Rev. Lett. **110**, 097204 (2013).

[27] Y. Yamaji, Y. Nomura, M. Kurita, R. Arita, and M. Imada, First-Principles Study of the Honeycomb-Lattice Iridates Na$_2$IrO$_3$ in the Presence of Strong Spin-Orbit Interaction and Electron Correlations, Phys. Rev. Lett. **113**, 107201 (2014).

[28] J. Reuther, R. Thomale, and S. Trebst, Finite-temperature phase diagram of the Heisenberg-Kitaev model, Phys. Rev. B **84**, 100406 (2011).

[29] I. Kimchi and Y.-Z. You, Kitaev-Heisenberg-J_2-J_3 model for the iridates A_2IrO$_3$, Phys. Rev. B **84**, 180407 (2011).

[30] V. M. Katukuri, S. Nishimoto, V. Yushankhai, A. Stoyanova, H. Kandpal, S. Choi, R. Coldea, I. Rousochatzakis, L. Hozoi, and J. van den Brink, Kitaev interactions between j=1/2 moments in honeycomb Na$_2$IrO$_3$ are large and ferromagnetic: insights from ab initio quantum chemistry calculations, New J. Phys. **16**, 013056 (2014).

[31] K. Foyevtsova, H. O. Jeschke, I. I. Mazin, D. I. Khomskii, and R. Valentí, *Ab initio* analysis of the tight-binding parameters and magnetic interactions in Na$_2$IrO$_3$, Phys. Rev. B **88**, 035107 (2013).

[32] Y. Sizyuk, C. Price, P. Wölfle, and N. B. Perkins, Importance of anisotropic exchange interactions in honeycomb iridates: Minimal model for zigzag antiferromagnetic order in Na$_2$IrO$_3$, Phys. Rev. B **90**, 155126 (2014).

[33] T. Suzuki, T. Yamada, Y. Yamaji, and S. Suga, Dynamical properties of the honeycomb-lattice iridates Na$_2$IrO$_3$, Phys. Rev. B **92**, 184411 (2015).

[34] A. Banerjee, C. Bridges, J.-Q. Yan, A. Aczel, L. Li, M. Stone, G. Granroth, M. Lumsden, Y. Yiu, J. Knolle, et al., Proximate Kitaev quantum spin liquid behaviour in a honeycomb magnet, Nat. Mater. (2016), 10.1038/nmat4604.

[35] H.-S. Kim and H.-Y. Kee, Crystal structure and magnetism in $\alpha - RuCl_3$: An *ab initio* study, Phys. Rev. B **93**, 155143 (2016).

[36] Y. Yamaji, T. Suzuki, T. Yamada, S. Suga, N. Kawashima, and M. Imada, Clues and criteria for designing a Kitaev spin liquid revealed by thermal and spin excitations of the honeycomb iridate Na$_2$IrO$_3$, Phys. Rev. B **93**, 174425 (2016).

[37] Y. Kamiya, Y. Kato, J. Nasu, and Y. Motome, Magnetic three states of matter: A quantum Monte Carlo study of spin liquids, Phys. Rev. B **92**, 100403 (2015).

[38] S. Sugiura and A. Shimizu, Thermal Pure Quantum States at Finite Temperature, Phys. Rev. Lett. **108**, 240401 (2012).

[39] S. Sugiura and A. Shimizu, Canonical Thermal Pure Quantum State, Phys. Rev. Lett. **111**, 010401 (2013).

[40] M. Hyuga, S. Sugiura, K. Sakai, and A. Shimizu, Thermal pure quantum states of many-particle systems, Phys. Rev. B **90**, 121110 (2014).

[41] Y. Yamaji, T. Misawa, S. Todo, K. Yoshimi, M. Kawamura, and N. Kawashima, https://github.com/QLMS/HPhi (unpublished).

[42] S. Mandal, S. Bhattacharjee, K. Sengupta, R. Shankar, and G. Baskaran, Confinement-deconfinement transition and spin correlations in a generalized Kitaev model, Phys. Rev. B **84**, 155121 (2011).

[43] H.-D. Chen and J. Hu, Exact mapping between classical and topological orders in two-dimensional spin systems, Phys. Rev. B **76**, 193101 (2007).

[44] X.-Y. Feng, G.-M. Zhang, and T. Xiang, Topological Characterization of Quantum Phase Transitions in a Spin-1/2 Model, Phys. Rev. Lett. **98**, 087204 (2007).

[45] H.-D. Chen and Z. Nussinov, Exact results of the Kitaev model on a hexagonal lattice: spin states, string and brane correlators, and anyonic excitations, J. Phys. A **41**, 075001 (2008).

[46] See Supplemental Material.

[47] J. Vidal, R. Thomale, K. P. Schmidt, and S. Dusuel, Self-duality and bound states of the toric code model in a transverse field, Phys. Rev. B **80**, 081104 (2009).

[48] C. Xu and J. E. Moore, Strong-Weak Coupling Self-Duality in the Two-Dimensional Quantum Phase Transition of $p + ip$ Superconducting Arrays, Phys. Rev. Lett. **93**, 047003 (2004).

[49] Z. Nussinov and E. Fradkin, Discrete sliding symmetries, dualities, and self-dualities of quantum orbital compass models and $p + ip$ superconducting arrays, Phys. Rev. B **71**, 195120 (2005).

[50] T. Tanaka and S. Ishihara, Dilution Effects in Two-Dimensional Quantum Orbital Systems, Phys. Rev. Lett. **98**, 256402 (2007).
[51] S. Wenzel and W. Janke, Monte Carlo simulations of the directional-ordering transition in the two-dimensional classical and quantum compass model, Phys. Rev. B **78**, 064402 (2008).
[52] J. G. Rau, E. K.-H. Lee, and H.-Y. Kee, Generic Spin Model for the Honeycomb Iridates beyond the Kitaev Limit, Phys. Rev. Lett. **112**, 077204 (2014).
[53] H. Rieger and N. Kawashima, Application of a continuous time cluster algorithm to the two-dimensional random quantum Ising ferromagnet, Eur. Phys. J. B **9**, 233 (1999).